journal

J. Am. Ceram. Soc., **96** [12] 3862–3867 (2013)
DOI: 10.1111/jace.12613

Low-Temperature Sinterable $(1-x)Ba_3(VO_4)_2$–$xLiMg_{0.9}Zn_{0.1}PO_4$ Microwave Dielectric Ceramics

Yang Lv, Ruzhong Zuo,† Ying Cheng, and Chen Zhang

Institute of Electro Ceramics & Devices, School of Materials Science and Engineering, Hefei University of Technology, Hefei 230009, China

The novel low-temperature sinterable $(1-x)Ba_3(VO_4)_2$–$xLiMg_{0.9}Zn_{0.1}PO_4$ microwave dielectric ceramics were prepared by cofiring the mixtures of pure-phase $Ba_3(VO_4)_2$ and $LiMg_{0.9}Zn_{0.1}PO_4$. The phase structure and grain morphology of the ceramics were evaluated using X-ray diffraction, Raman spectra, and scanning electron microscopy. The results indicated that $Ba_3(VO_4)_2$ and $LiMg_{0.9}Zn_{0.1}PO_4$ phases can well coexist in the sintered body. Nevertheless, a small amount of $LiZnPO_4$ and some vanadate phases with low melting points were observed, which not only can influence the microwave dielectric properties of the ceramic but also can obviously improve the densification behavior at a relatively low sintering temperature. The near-zero temperature coefficients of the resonant frequency (τ_f) could be achieved by adjusting the relative content of the two phases owing to their opposite τ_f values and simultaneously a desirable quality factor $Q \times f$ value can be maintained. No chemical reaction between the matrix ceramic phase and Ag took place after sintering at 800°C for 4 h. The ceramics with 45 vol% $LiMg_{0.9}Zn_{0.1}PO_4$ can be well sintered at only 800°C and exhibit excellent microwave dielectric properties of $\varepsilon_r \sim 10$, $Q \times f \sim 64\,500$ GHz, and $\tau_f \sim -2.1$ ppm/°C, thus showing a great potential as a low-permittivity low-temperature cofired microwave dielectric material.

I. Introduction

With the development of the modern communication technologies toward higher frequencies, multilayer chip microwave devices such as filters and GPS patch antennas have attracted much more attention. The rapid growth of the consumer electronic market requires new advanced integration, packaging, and interconnection technologies to realize the microwave devices with the high-miniaturization, high-reliability, and multifunctional performance. The low-temperature cofired ceramic (LTCC) technology can provide a visible solution for the material and processing to enable the requirement of the microwave devices. To be applicable to the higher frequency region, the microwave devices must have a low dielectric loss and high-temperature stability. In addition, the microwave dielectric ceramics based on the LTCC technology not only should be densified below the melting point (961°C) of Ag electrode but also have a low dielectric constant (ε_r), a near-zero temperature dependence of the resonant frequency (τ_f), and a high-quality factor ($Q \times f$).[1–4]

Some ceramics such as $Mg_4Nb_2O_9$, Zn_2SiO_4, and Mg_2SiO_4 exhibit a low ε_r and a giant $Q \times f$ value, however, their high sintering temperatures and large negative τ_f values are far beyond the requirement of the LTCC microwave devices.[5,6] One of the most effective ways to tailor the negative τ_f value to near zero is to add the opposite τ_f value material, such as $MgTiO_3$–$CaTiO_3$ and Mg_2SiO_4–$Ba_3(VO_4)_2$ ceramic systems.[7,8] The common methods to decrease the sintering temperature are involved in synthesizing ultrafine precursor powders by wet chemical processing or mixing with low-melting-point additives. However, the wet chemical processing was not suitable in practice due to its complicated and costly synthesis procedures. The addition of low-melting-point additives would usually deteriorate the microwave dielectric properties of the matrix ceramics seriously.[9,10] Another way to achieve high-performance LTCC microwave dielectric materials is to employ some new material systems with excellent microwave dielectric properties and a low sintering temperature. Some phosphates with low-cost, easily processable, lightweight characteristics were reported to be very promising for LTCC applications. Liu *et al.* reported that the new phosphate $Li_3Bi_2P_3O_{12}$ ceramic sintered at extremely low temperature (~725°C) has good microwave dielectric properties of $\varepsilon_r \sim 15$ and $Q \times f \sim 27\,000$ GHz.[11] However, the large negative τ_f of −130 ppm/°C precludes its immediate application for LTCCs. Thomas *et al.* reported that $LiMgPO_4$ sintered at ~950°C exhibits a low-permittivity ε_r of ~6.6, a high $Q_u \times f$ of 79100 GHz, and a τ_f value of −55 ppm/°C.[12] Its quality factor could be further boosted when 10% Zn^{2+} was substituted for Mg^{2+} ($Q_u \times f = 99\,700$ GHz), however, its τ_f value became more negative (−60 ppm/°C).[13] The similar ionic radius between Mg^{2+} (0.72 Å, CN = 6) and Zn^{2+} (0.74 Å, CN = 6) would make Zn^{2+} solute into the crystal structure of $LiMgPO_4$ to a certain degree. As a result, the orthorhombic $LiMg_{0.9}Zn_{0.1}PO_4$ solid solution was formed without any secondary phase. Nevertheless, the $LiMg_{0.9}Zn_{0.1}PO_4$ ceramic will be a promising low-permittivity LTCC material if its negative τ_f value can be tailored to be near zero.

$Ba_3(VO_4)_2$ ceramic was reported to have a large positive τ_f value (52 ppm/°C) and good microwave dielectric properties (ε_r~14, $Q \times f \sim 42\,000$ GHz) as it was sintered at ~1100°C. Compared with other microwave dielectric materials with positive τ_f values such as TiO_2, $CaTiO_3$, and $SrTiO_3$, relatively good microwave dielectric properties make $Ba_3(VO_4)_2$ be usually used as a τ_f-tailoring material, such as $Ba_3(VO_4)_2$–$BaWO_4$ and $Ba_3(VO_4)_2$–$CaWO_4$ systems.[14,15] Moreover, its relatively low sintering temperature allows $Ba_3(VO_4)_2$-based microwave dielectric ceramic systems to be easily sintered. So, one can expect that a diphasic microwave dielectric ceramic with a near-zero τ_f value, a high $Q \times f$ value, and a low sintering temperature would be obtained by combining $Ba_3(VO_4)_2$ with $LiMg_{0.9}Zn_{0.1}PO_4$. In this work, the $(1-x)Ba_3(VO_4)_2$–$xLiMg_{0.9}Zn_{0.1}PO_4$ ceramics were prepared and their low-temperature sintering behavior, microstructure, and microwave dielectric properties were investigated systematically. Moreover, the chemical compatibility of the material with Ag electrode was also studied.

P. Davies—contributing editor

Manuscript No. 33105. Received April 27, 2013; approved August 12, 2013.
†Author to whom correspondence should be addressed. e-mail: piezolab@hfut.edu.cn

II. Experimental Procedure

High-purity (>99%) powders of $BaCO_3$, V_2O_5, Li_2CO_3, $(MgCO_3)_4{\cdot}Mg(OH)_2{\cdot}5H_2O$, ZnO (nanosized), and $NH_4H_2PO_4$ were used as raw materials in this study. $Ba_3(VO_4)_2$ and $LiMg_{0.9}Zn_{0.1}PO_4$ were first synthesized individually via a conventional solid-state reaction method by calcining their respective stoichiometric powder mixtures in the temperature range 750°C–800°C for 4 h. Subsequently, $(1-x)Ba_3(VO_4)_2$–$xLiMg_{0.9}Zn_{0.1}PO_4$ (x = 0.2–0.65, in vol%) powder mixtures were prepared by mixing the as-calcined $Ba_3(VO_4)_2$ and $LiMg_{0.9}Zn_{0.1}PO_4$ powders. The mixtures were then ball-milled for 8 h using zirconia balls in alcohol medium. The granulated powders were subsequently pressed into cylinders with dimensions of 10 mm in diameter and 7–8 mm in height. These specimens were first heated at 550°C in air for 4 h to burn out the organic binder, and then sintered in air in the temperature range 770°C–880°C for 2–6 h. To study the chemical compatibility with Ag, ceramic samples were ground and mixed with 20 wt% Ag powder, and then sintered at 800°C for 4 h.

The bulk densities of the sintered ceramics were measured by the Archimedes method. The crystal structure of the samples was investigated by X-ray diffraction (XRD; D/Max2500V, Rigaku, Tokyo, Japan) using Cu$K\alpha$ radiation. The microstructure of the sintered samples was observed using a scanning electron microscope (SEM; JSM-6490LV, JEOL, Tokyo, Japan) equipped with an energy dispersive spectrometer (EDS). The Raman spectrum was collected at room temperature using a Raman microscope (633 nm, LabRAM, HR800, Longjumeau Cedex, Nantes, France). Microwave dielectric properties were measured using the Hakki–Coleman method and the $TE_{01\delta}$-shield cavity method with a Network Analyzer (N5230C; Agilent, Palo Alto, CA).[16] The dielectric loss (tan δ) was calculated using the software provided by the $TE_{01\delta}$-shield cavity supplier (Resonant cavity; QWED, Warsaw, Poland). The Q values were calculated from the tan δ values in accordance with the equation $Q = 1/\tan\delta$. The τ_f value of the samples was measured in the temperature range from 20°C to 80°C. It can be calculated by the following relationship:

$$\tau_f = \frac{f_2 - f_1}{f_1(T_2 - T_1)} \quad (1)$$

where f_1 and f_2 represent the resonant frequencies at T_1 and T_2, respectively.

III. Results and Discussion

Figure 1 shows the XRD patterns of $(1-x)Ba_3(VO_4)_2$–$xLiMg_{0.9}Zn_{0.1}PO_4$ (x = 0.4–0.65) ceramics sintered at 800°C for 4 h. All the main peaks can be indexed by $Ba_3(VO_4)_2$ (JCPDS #25-1192) and $LiMgPO_4$ phase (JCPDS #32-0574), illustrating that the as-sintered ceramic is basically composed of two main phases. The addition of a small amount of Zn^{2+} did not change the crystal structure of $LiMPO_4$ as well. However, a small amount of secondary phases appearing in the composition range x = 0.65–0.50 can be indexed by $LiZnPO_4$ (JCPDS # 84-2136). The space group of $Ba_3(VO_4)_2$ is $R\bar{3}2/m$, with the V^{5+} ions located in the center of tetrahedral [VO_4] units linked by sixfold and tenfold coordinate Ba^{2+} ions.[8] $LiMg_{0.9}Zn_{0.1}PO_4$ belongs to the ordered olivine-type structure, which is orthorhombic, with a space group *Pmnb*, and contains tetrahedral PO_4 and octahedral LiO_6 and MgO_6 groups. It should be noted that $LiZnPO_4$ exhibits a monoclinic structure and belongs to the *Cc* space group.[12] The large difference in the crystal structure of both phases might be responsible for the formation of the minimum secondary phases owing to their limited solubility. Moreover, it can be seen that the concentration of the $LiZnPO_4$ phase decreased obviously with increasing the content of $Ba_3(VO_4)_2$ and it further vanished when the $Ba_3(VO_4)_2$ content was above 50%. In addition, a little secondary phase appearing at 28.8° and 29.2° in the composition range x = 0.65–0.4 could be indexed using the standard pattern of $Zn_3(VO_4)_2$ (JCPDS # 19-1468), which can be also ascribed to the reaction between $Ba_3(VO_4)_2$ and $LiMg_{0.9}Zn_{0.1}PO_4$ phases.

Figure 2 shows the XRD patterns of $0.55Ba_3(VO_4)_2$–$0.45LiMg_{0.9}Zn_{0.1}PO_4$ ceramics sintered at various temperatures for 4 h. It can be found that the peak intensity of $Zn_3(VO_4)_2$ secondary phase decreased and the peak position was slightly shifted to lower diffraction angles as the sintering temperature increased from 770°C to 860°C, as confirmed by the inset of Fig. 2. It was reported that the $Zn_3(VO_4)_2$ compound can decompose into other vanadates, such as $Zn_2V_2O_7$ compound starting from ~830°C (see the inset of Fig. 2). It can form a low-melting-point liquid phase as the temperature was increased to ~855°C.[17] Due to the emergence of vanadate secondary phases with low melting points, the $Ba_3(VO_4)_2$–$LiMg_{0.9}Zn_{0.1}PO_4$ ceramics are expected to be sintered at a rather low temperature (below 860°C). In addition,

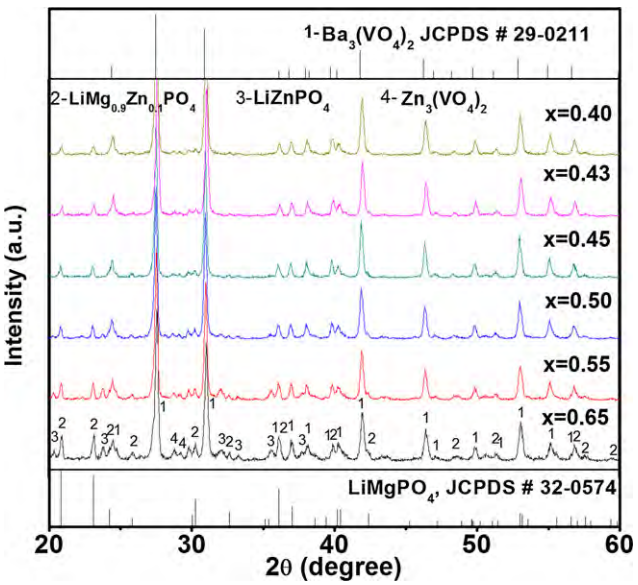

Fig. 1. XRD patterns of $(1-x)Ba_3(VO_4)_2$–$xLiMg_{0.9}Zn_{0.1}PO_4$ (x = 0.40–0.65) ceramics sintered at 800°C for 4 h, as compared to the standard patterns of $Ba_3(VO_4)_2$ and $LiMgPO_4$.

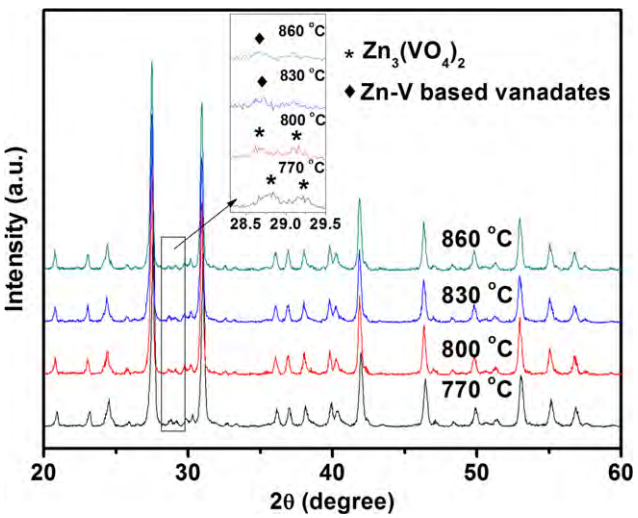

Fig. 2. XRD patterns of $0.55Ba_3(VO_4)_2$–$0.45LiMg_{0.9}Zn_{0.1}PO_4$ ceramics sintered at various temperatures for 4 h.

the effect of the sintering duration time on the XRD patterns of $0.55Ba_3(VO_4)_2$–$0.45LiMg_{0.9}Zn_{0.1}PO_4$ ceramics sintered at 800°C is shown in Fig. 3, in which the XRD pattern of the mixture of the $x = 0.45$ ceramic powder and 20 wt% Ag sintered at 800°C for 4 h is also included for comparison. On one hand, it is obvious that the phase compositions of the sintered ceramics are not sensitive to the sintering time at 800°C because the diffraction peaks do not obviously change with time. This result means that the sintering time may influence the sample density, but do not greatly deteriorate the reaction of $Ba_3(VO_4)_2$ and $0.45LiMg_{0.9}Zn_{0.1}PO_4$. On the other hand, for the cofired samples of the $x = 0.45$ matrix composition with Ag powder, besides peaks of the ceramic sample (see Fig. 2) and Ag (JCPDS #04-0783), there are no additional peaks in the XRD patterns to reflect a secondary phase formed, implying that $0.55Ba_3(VO_4)_2$–$0.45LiMg_{0.9}Zn_{0.1}PO_4$ ceramic does not react with Ag at the sintering temperature.

The Raman spectra of the $Ba_3(VO_4)_2$–$LiMg_{0.9}Zn_{0.1}PO_4$ ceramics are shown in Fig. 4. The Raman bands of

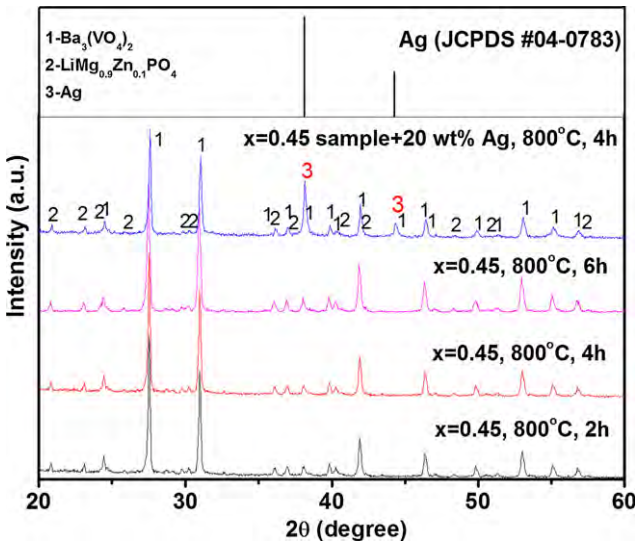

Fig. 3. XRD patterns of $0.55Ba_3(VO_4)_2$–$0.45LiMg_{0.9}Zn_{0.1}PO_4$ ceramics sintered at 800°C for different hours and the cofired sample of the $x = 0.45$ ceramic and 20 wt% Ag at 800°C for 4 h.

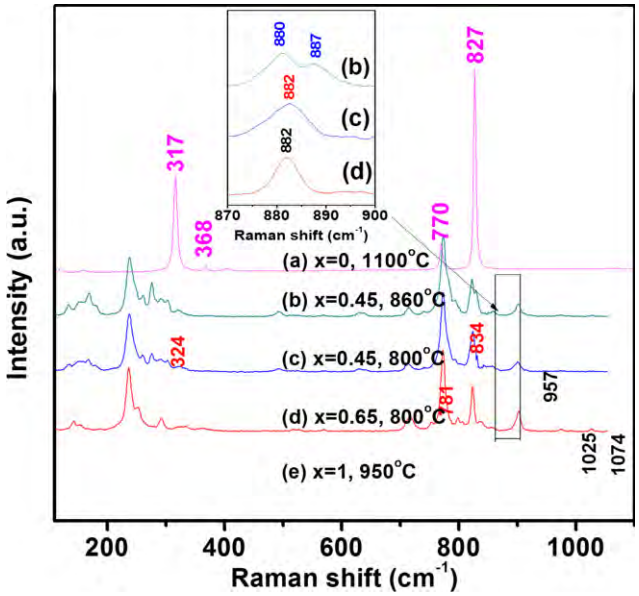

Fig. 4. Raman spectra of $(1 - x)Ba_3(VO_4)_2$–$xLiMg_{0.9}Zn_{0.1}PO_4$ ceramics sintered at various temperatures.

$Ba_3(VO_4)_2$ were distributed in three well-separated frequency regions corresponding to the internal stretching of $[VO_4]$ modes (V–O stretching modes, 850–750 cm^{-1}), the internal bending of $[VO_4]$ modes (O–V–O bending modes, 450–300 cm^{-1}), and translational and rotational modes of the $[VO_4]$ units mixed with the Ba^{2+} displacements (250–120 cm^{-1}).[18] The main Raman-active modes of $LiMg_{0.9}Zn_{0.1}PO_4$ at 957, 1025, and 1074 cm^{-1} can be ascribed to the stretching and bending vibrations of its polyhedrons, which contain tetrahedral $[PO_4]$, octahedral $[LiO_6]$, and $[MgO_6]$.[19] According to the Raman spectra of the pure-phase $Ba_3(VO_4)_2$ and $LiMg_{0.9}Zn_{0.1}PO_4$, all the Raman-active modes in the $(1 - x)Ba_3(VO_4)_2$–$xLiMg_{0.9}Zn_{0.1}PO_4$ ($x = 0.40$–0.65) ceramics can be identified by these two phases. It can be seen that the Raman band located at 882 cm^{-1} in the composition range $x = 0.4$–0.65 should be attributed to the $Zn_3(VO_4)_2$ phase. However, it was spilt into double bands corresponding to the vibration bands of 880 and 887 cm^{-1} (see the inset of Fig. 4) when the sintering temperature was raised up to 860°C, which can be attributed to the decomposition products of $Zn_3(VO_4)_2$, such as the $Zn_2V_2O_7$ and $Zn_4V_2O_9$ compounds. Raman results indicated that $Ba_3(VO_4)_2$–$LiMg_{0.9}Zn_{0.1}PO_4$ ceramics have been generally formed, in which the change in the crystal structure and phase compositions keep consistency with that of the XRD results.

Figure 5 shows the SEM images and EDS result of $(1 - x)Ba_3(VO_4)_2$–$xLiMg_{0.9}Zn_{0.1}PO_4$ ($x = 0.4$–0.65) ceramics sintered at various temperatures. It can be noted that all the specimens exhibit a bimodal grain size distribution and are composed of two kinds of grains with different contents. The result of EDS analysis [Fig. 5(f)] shows that big and light grains [marked 1 in Fig. 5(e)] mainly contain Ba, V, and O elements in an approximate molar ratio of Ba:V:O = 3:2:8, and small and dark grains [marked 2 in Fig. 5(e)] are dominantly composed of Mg, Zn, P, and O elements, in which the Li element belongs to the ultralight elements so that it cannot be detected by EDS. From the EDS results, it can be also found that some Ba^{2+} and V^{5+} ions were detected in the grain of $LiMg_{0.9}Zn_{0.1}PO_4$, and Mg^{2+}, Zn^{2+}, and P^{5+} ions were also detected in the grain of $Ba_3(VO_4)_2$, probably because of the ions diffusion between two phases. This is because the crystal structure of $LiMg_{0.9}Zn_{0.1}PO_4$ is not very stable, such that part of Zn^{2+} ions can leave away from the Mg(Zn)–O site as it was reacted with $Ba_3(VO_4)_2$. As a result, some Zn^{2+} ions exist as $LiZnPO_4$ secondary phases, and some other Zn^{2+} ions replace Ba^{2+} ions to form $Zn_3(VO_4)_2$ compound. A small amount of Ba^{2+} ions can fill in the vacancies of $LiMgPO_4$ lattices by occupying the Mg–O site. Figures. 5(a), (c), and (e) show the grain morphology of $0.55Ba_3(VO_4)_2$–$0.45LiMg_{0.9}Zn_{0.1}PO_4$ ceramics sintered at 770°C, 800°C, and 860°C, respectively. It can be observed that the grain size of the ceramics increases with increasing the sintering temperature. The low-melting-point Zn–V-based secondary phases can form liquid phases during sintering, which can speed up the particle rearrangement in the early period of sintering and the mass transportation in the middle period of sintering. However, the grain growth can be simultaneously promoted. The enhanced grain growth behavior tends to lower the sintering driving force for densification, so that the sample density decreases as the sintering temperature is too high. As a result, samples sintered at 800°C have a relatively high density without obvious porosity and exhibit a uniform microstructure. From Fig. 5(e), it can be seen that some remaining pores are visible and the sample density starts to decrease as the sintering temperature increases up to 860°C.

Figure 6 shows the relative density and ε_r values of $(1 - x)Ba_3(VO_4)_2$–$xLiMg_{0.9}Zn_{0.1}PO_4$ ($x = 0.2$–0.65) ceramics as a function of the sintering temperature. It can be seen that the addition of $LiMg_{0.9}Zn_{0.1}PO_4$ can effectively reduce the sintering temperature of the ceramics compared to the

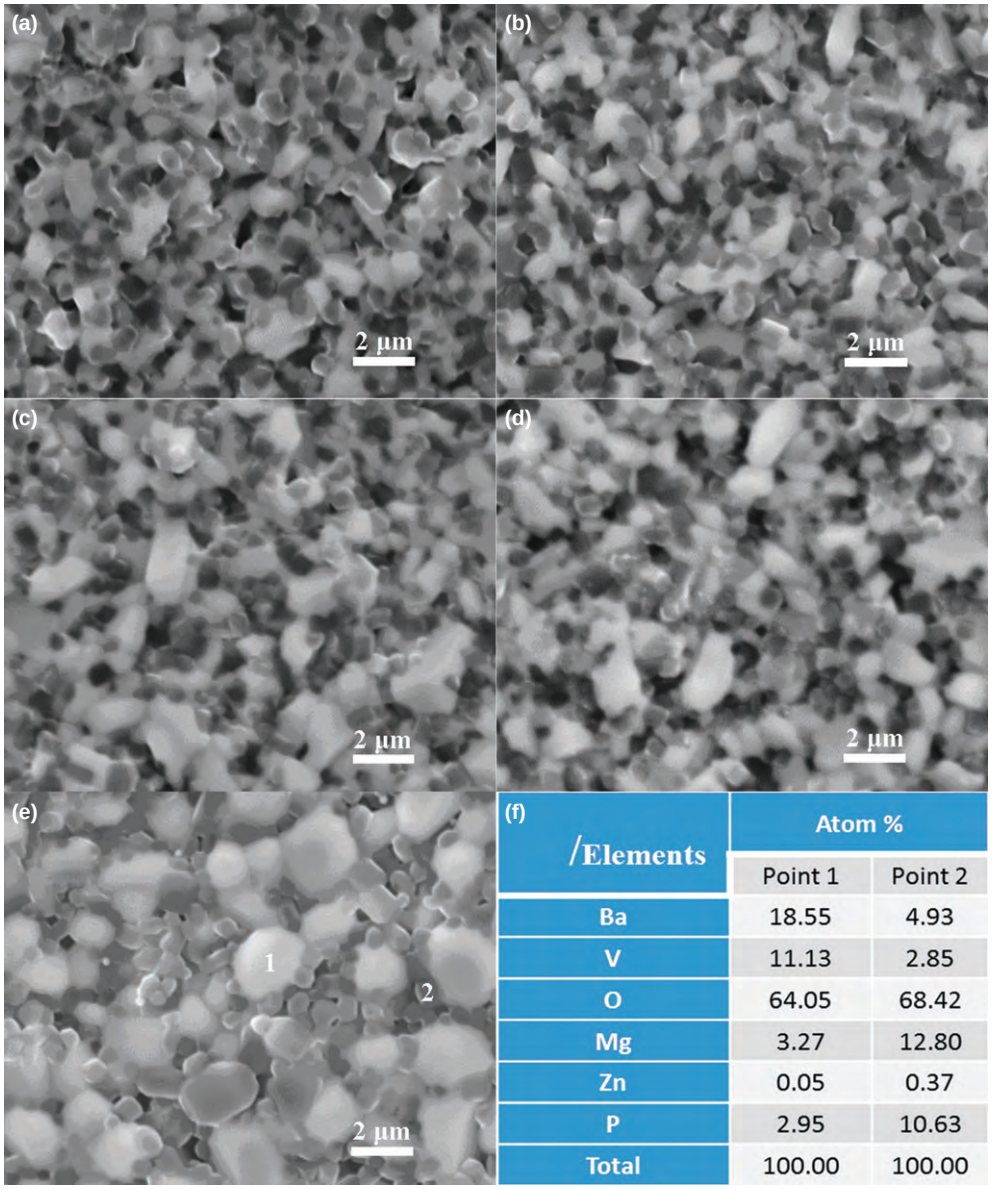

(f)

/Elements	Atom %	
	Point 1	Point 2
Ba	18.55	4.93
V	11.13	2.85
O	64.05	68.42
Mg	3.27	12.80
Zn	0.05	0.37
P	2.95	10.63
Total	100.00	100.00

Fig. 5. SEM images of the $(1-x)Ba_3(VO_4)_2$–$xLiMg_{0.9}Zn_{0.1}PO_4$ ceramics: (a) $x = 0.45$, at 770°C, (b) $x = 0.40$, at 800°C, (c) $x = 0.45$, at 800°C, (d) $x = 0.55$, at 800°C, (e) $x = 0.45$, at 860°C, and (f) EDS result for $x = 0.45$, at 860°C.

single-phase $Ba_3(VO_4)_2$ ceramics. The $Ba_3(VO_4)_2$–$LiMg_{0.9}Zn_{0.1}PO_4$ ceramic sample can be well densified in the temperature range 800°C–830°C. Generally, the relative density of all ceramic samples decreases with further increasing the sintering temperature. The optimum sintering temperature of each sample slightly decreases with increasing the $LiMg_{0.9}Zn_{0.1}PO_4$ content. The ε_r values of the ceramics varying with the sintering temperature show a similar tendency to the sample density, as the ε_r value is usually strongly dependent on density. It can be found that the ε_r value of the $(1-x)Ba_3(VO_4)_2$–$xLiMg_{0.9}Zn_{0.1}PO_4$ ceramic is approximately in the range 7–12, which is roughly between those of the single-phase $Ba_3(VO_4)_2$ and $LiMg_{0.9}Zn_{0.1}PO_4$ ceramic. Nevertheless, the experimental ε_r value of the $Ba_3(VO_4)_2$–$LiMg_{0.9}Zn_{0.1}PO_4$ ceramic indicated that the formation of a small amount of secondary phases such as $LiZnPO_4$ and $Zn_3(VO_4)_2$ secondary phases has an negligible effect on the dielectric constant because these secondary phases were reported similar ε_r values to both of $Ba_3(VO_4)_2$ and $LiMg_{0.9}Zn_{0.1}PO_4$ ceramics,[13,20] although the temperature for the optimum densification was decreased.

Figure 7 shows the $Q \times f$ values of $(1-x)Ba_3(VO_4)_2$–$xLiMg_{0.9}Zn_{0.1}PO_4$ ($x = 0.2$–0.65) ceramics as a function of the $LiMg_{0.9}Zn_{0.1}PO_4$ content, x. As the single-phase $LiMg_{0.9}Zn_{0.1}PO_4$ has a much bigger $Q \times f$ value (99 700 GHz) than that of the $Ba_3(VO_4)_2$ ceramic ($Q \times f = 42\,000$ GHz), the $Q \times f$ value of the $(1-x)Ba_3(VO_4)_2$–$xLiMg_{0.9}Zn_{0.1}PO_4$ ceramics should generally increase with increasing the content of $LiMg_{0.9}Zn_{0.1}PO_4$. The $Q \times f$ value of the $(1-x)Ba_3(VO_4)_2$–$xLiMg_{0.9}Zn_{0.1}PO_4$ ceramics is not only related to the relative content of both phases but also is closely associated with imperfections such as porosity, grain boundaries, microcracks, and impurities.[21] As a result, the $Q \times f$ value started to decrease as the $LiMg_{0.9}Zn_{0.1}PO_4$ content was further increased. As the ceramic was sintered in the temperature range 770°C–880°C, the $Q \times f$ value first increased with increasing the $LiMg_{0.9}Zn_{0.1}PO_4$ content, and then decreased when the x value was larger than ~0.43. The decreased $Q \times f$ values of the ceramic with increasing the $LiMg_{0.9}Zn_{0.1}PO_4$ content should be mainly ascribed to the presence of some $LiZnPO_4$ and $Zn_3(VO_4)_2$ secondary phases in the sintered ceramics because both $LiZnPO_4$ ($Q \times f \sim 40\,000$ GHz)[13] and $Zn_3(VO_4)_2$ ($Q \times f \sim 20\,000$ GHz)[20] show much smaller $Q \times f$ values. As the sample was sintered in the temperature range 860°C–880°C, the $Q \times f$ value became much smaller than that of the sample sintered below 860°C. The possible reason might be also ascribed to the slight decrease in the sample

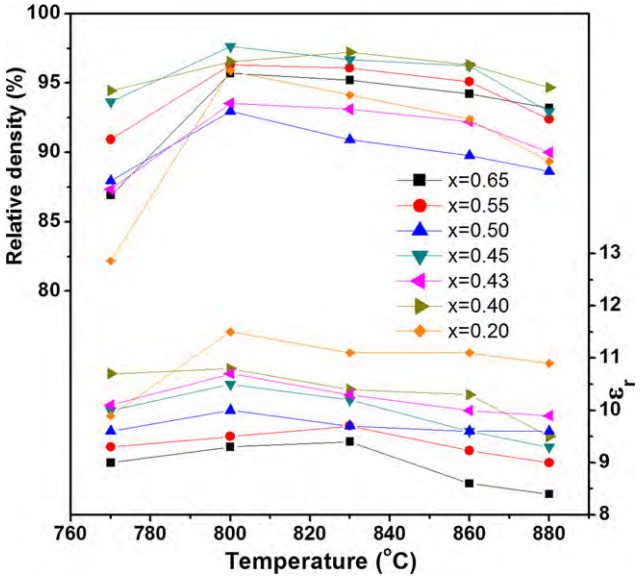

Fig. 6. Bulk density and ε_r values of the $(1-x)Ba_3(VO_4)_2$–$xLiMg_{0.9}Zn_{0.1}PO_4$ ceramics as a function of the sintering temperature.

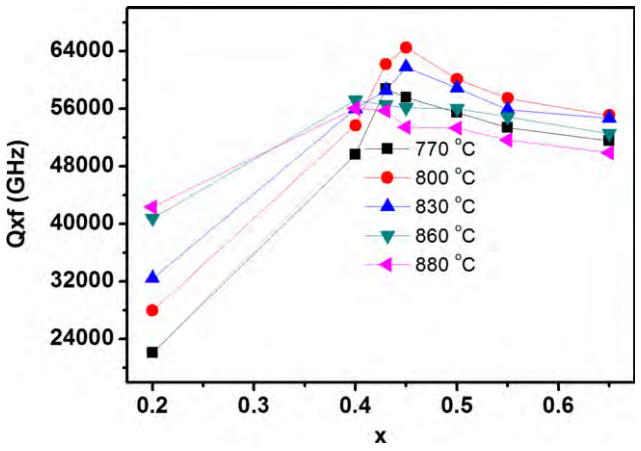

Fig. 7. The $Q \times f$ values of the $(1-x)Ba_3(VO_4)_2$–$xLiMg_{0.9}Zn_{0.1}PO_4$ ceramics sintered at different temperatures for 4 h.

density. Moreover, we also found that the sintering duration time shows only a little influence on the ε_r and $Q \times f$ values as the sample was sintered at 800°C for longer than 4 h, because the formation of impurity phases is not sensitive to the sintering time (Fig. 3), compared with the sintering temperature (Fig. 2), and the maximum sample density has been almost reached after 4 h.

The τ_f values of the $(1-x)Ba_3(VO_4)_2$–$xLiMg_{0.9}Zn_{0.1}PO_4$ (x = 0.2–0.65) ceramics as a function of the sintering temperature and the $LiMg_{0.9}Zn_{0.1}PO_4$ content are shown in Fig. 8. The τ_f value increased monotonically from −33 ppm/°C to 23.3 ppm/°C as x decreased from 0.65 to 0.2 at different sintering temperatures. The inset of Fig. 8 illustrates the calculated and measured τ_f values for different samples sintered at 800°C. The sintered $(1-x)Ba_3(VO_4)_2$–$xLiMg_{0.9}Zn_{0.1}PO_4$ ceramics could be roughly considered as diphasic ceramics because the concentration of secondary phases formed during sintering is very low and is difficult to know clearly. Therefore, the calculated τ_f values can be obtained by the following equation:

$$\tau_f = V_1 \cdot \tau_{f1} + V_2 \cdot \tau_{f2} \quad (2)$$

where V is the volume fraction of each phase. The subscripts 1 and 2 stand for $Ba_3(VO_4)_2$ and $LiMg_{0.9}Zn_{0.1}PO_4$ phases,

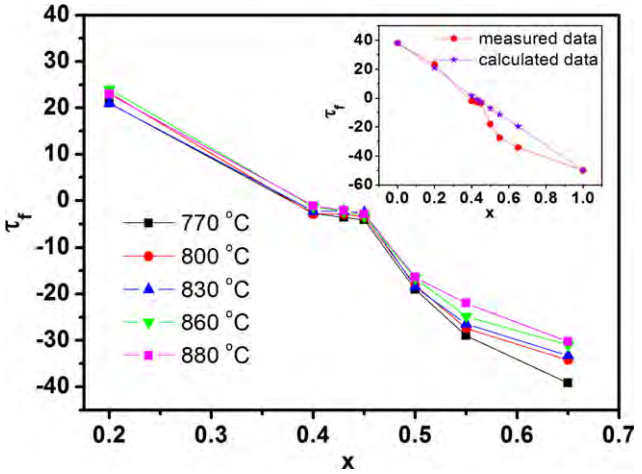

Fig. 8. The τ_f values of the $(1-x)Ba_3(VO_4)_2$–$xLiMg_{0.9}Zn_{0.1}PO_4$ ceramics sintered at different temperatures for 4 h.

respectively. It can be found that the calculated values are almost equal to the measured values as x is less than 0.45, and then the discrepancy of both values increases as x increases from 0.5 to 0.65. This difference might be attributed to the existence of the $LiZnPO_4$ and $Zn_3(VO_4)_2$ phase whose concentrations vary with the change in x. It also can be found that the measured τ_f value was smaller than the calculated ones (see the inset of Fig. 8), which can be explained by the emergence of $LiZnPO_4$ and $Zn_3(VO_4)_2$ phases. It has been reported that the τ_f value of $LiZnPO_4$ was about −80 ppm/°C[13] and the τ_f value of $Zn_3(VO_4)_2$ ceramic sintered at 800°C was approximately −120 ppm/°C.[20] Despite the content of the $Zn_3(VO_4)_2$ secondary phase would be very low, the τ_f value of the ceramics was obviously reduced. Nevertheless, the $0.55Ba_3(VO_4)_2$–$0.45LiMg_{0.9}Zn_{0.1}PO_4$ ceramics sintered at 800°C exhibit a zero-near τ_f value of −2.1 ppm/°C. In addition, this composition also has an excellent $Q \times f$ value of 64 500 GHz and a low ε_r value of 10. Therefore, it can be believed that $(1-x)Ba_3(VO_4)_2$–$xLiMg_{0.9}Zn_{0.1}PO_4$ ceramics could be a good low-permittivity LTCC microwave dielectric material as the $LiMg_{0.9}Zn_{0.1}PO_4$ content is appropriately adjusted.

IV. Conclusions

The $Ba_3(VO_4)_2$–$LiMg_{0.9}Zn_{0.1}PO_4$ ceramics were successfully manufactured via a conventional solid-state reaction method. The phase structure, densification behavior, and microwave dielectric properties of the ceramics were investigated as a function of the sintering temperature and time, and the relative content of each phase. The low-temperature sinterability and desirable microwave dielectric properties can be achieved by appropriately adjusting the relative content of $Ba_3(VO_4)_2$ and $LiMg_{0.9}Zn_{0.1}PO_4$ phases. The experimental results demonstrate that the ceramics with 45% $LiMg_{0.9}Zn_{0.1}PO_4$ can be well densified at 800°C, and exhibit excellent microwave dielectric properties of $\varepsilon_r \sim 10$, $Q \times f \sim 64\,500$ GHz, and $\tau_f \sim -2.1$ ppm/°C, and good chemical compatibility with Ag electrode.

Acknowledgments

Financial support from the Natural Science Foundation Anhui Province (Grant No. 1108085J14) and the National Natural Science Foundation of China (Grant No. 51272060) is gratefully acknowledged.

References

[1]H. Ogawa, A. Yokoi, R. Umemura, and A. Kan, "Microwave Dielectric Properties of $Mg_3(VO_4)_2$-$XBa_3(VO_4)_2$ Ceramics for LTCC with Near Zero Temperature Coefficient of Resonant Frequency," *J. Eur. Ceram. Soc.*, **27**, 3099–104 (2007).

[2]W. Lei, W. Z. Lu, D. Liu, and J. H. Zhu, "Phase Evolution and Microwave Dielectric Properties of $(1-x)ZnAl_2O_4$-XMg_2TiO_4 Ceramics," *J. Am. Ceram. Soc.*, **92**, 105–9 (2009).

[3]H. F. Zhou, X. L. Chen, L. Fang, X. B. Liu, and Y. L. Wang, "Microwave Dielectric Properties of $LiBiW_2O_8$ Ceramics with Low Sintering Temperature," *J. Am. Ceram. Soc.*, **93**, 3976–9 (2010).

[4]S. H. Kweon, M. R. Joung, J. S. Kim, B. Y. Kim, S. Nahm, J. H. Paik, Y. S. Kim, and T. Y. Sung, "Low Temperature Sintering and Microwave Dielectric Properties of B_2O_3-Added $LiAlSiO_4$ Ceramic," *J. Am. Ceram. Soc.*, **94**, 1995–8 (2011).

[5]A. Kan, H. Ogawa, A. Yokoi, and Y. Nakamura, "Crystal Structural Refinement of Corundum-Structured $A_4M_2O_9$ (A=Co and Mg, M=Nb and Ta) Microwave Dielectric Ceramics by High-Temperature X-ray Powder Diffraction," *J. Eur. Ceram. Soc.*, **27**, 2977–81 (2007).

[6]J. S. Kim, N. H. Nguyen, J. B. Lim, D. S. Paik, S. Nahm, J. H. Paik, J. H. Kim, and H. J. Lee, "Low-Temperature Sintering and Microwave Dielectric Properties of the Zn_2SiO_4 Ceramics," *J. Am. Ceram. Soc.*, **91**, 671–4 (2008).

[7]L. Li, X. M. Chen, and X. C. Fan, "Microwave Dielectric Characteristics and Finite Element Analysis of $MgTiO_3$-$CaTiO_3$ Layered Dielectric Resonators," *J. Eur. Ceram. Soc.*, **26**, 3265–71 (2006).

[8]S. Q. Meng, Z. X. Yue, H. Zhuang, F. Zhao, and L. T. Li, "Microwave Dielectric Properties of $Ba_3(VO_4)_2$-Mg_2SiO_4 Composite Ceramics," *J. Am. Ceram. Soc.*, **93**, 359–61 (2010).

[9]Y. Z. Hao, Q. L. Zhang, J. Zhang, C. R. Xin, and H. Yang, "Enhanced Sintering Characteristics and Microwave Dielectric Properties of Li_2TiO_3 Due to Nano-Size and Nonstoichiometry Effect," *J. Mater. Chem.*, **22**, 23885–92 (2012).

[10]M. R. Joung, J. S. Kim, M. E. Song, J. H. Choi, J. W. Sun, S. Nahm, J. H. Paik, and B. H. Choi, "Effect of Li_2CO_3 Addition on the Sintering Temperature and Microwave Dielectric Properties of $Mg_2V_2O_7$ Ceramics," *J. Am. Ceram. Soc.*, **92**, 2151–4 (2009).

[11]X. B. Liu, H. F. Zhou, L. Fang, X. L. Chen, W. Wang, C. Wang, and F. He, "Novel Series of Low-Firing Microwave Dielectric Ceramics: $(1-x)Li_3Bi_2P_3O_{12}$-$XTiO_2$," *J. Am. Ceram. Soc.*, **95**, 3357–9 (2012).

[12]D. Thomas and M. T. Sebastian, "Temperature-Compensated $LiMgPO_4$: A New Glass-Free Low-Temperature Cofired Ceramic," *J. Am. Ceram. Soc.*, **93**, 3828–31 (2010).

[13]D. Thomas and M. T. Sebastian, "Effect of Zn^{2+} Substitution on the Microwave Dielectric Properties of $LiMgPO_4$ and the Development of a New Temperature Stable Glass Free LTCC," *J. Eur. Ceram. Soc.*, **32**, 2359–64 (2012).

[14]H. Zhuang, Z. X. Yue, S. Q. Meng, F. Zhao, and L. T. Li, "Low-Temperature Sintering and Microwave Dielectric Properties of $Ba_3(VO_4)_2$-$BaWO_4$ Ceramic Composites," *J. Am. Ceram. Soc.*, **91**, 3738–41 (2008).

[15]Y. Lv and R. Z. Zuo, "Microstructure and Microwave Dielectric Properties of Low-Temperature Sinterable $(1-x)Ba_3(VO_4)_2$-$XCaWO_4$ Composite Ceramics," *J. Mater. Sci.: Mater. Electron.*, **24**, 1225–30 (2013).

[16]B. W. Hakki and P. D. Coleman, "A Dielectric Resonant Method of Measuring Inductive Capacities in the Millimeter Range," *IEEE Trans. Microwave Theory Technol.*, **8**, 402–10 (1960).

[17]M. Kurzawa, I. Rychlowska-Himmel, M. Bosacka, and A. Blonska-Tabero, "Reinvestigation of Phase Equilibrian in the V_2O_5-ZnO System," *J. Therm. Anal. Calorim.*, **64**, 1113–9 (2001).

[18]A. Grzechnik and P. F. McMillan, "High Pressure Behavior of $Sr_3(VO_4)_2$ and $Ba_3(VO_4)_2$," *J. Solid State Chem.*, **132**, 156–62 (1997).

[19]B. Ellis, W. H. Kan, W. R. M. Makahnouk, and L. F. Nazar, "Synthesis of Nanocrystals and Morphology Control of Hydrothermally Prepared $LiFePO_4$," *J. Mater. Chem.*, **17**, 3248–54 (2007).

[20]R. Umemura, H. Ogawa, and A. Kan, "Low Temperature Sintering and Microwave Dielectric Properties of $(Mg_{3-x}Zn_x)(VO_4)_2$ Ceramics," *J. Eur. Ceram. Soc.*, **26**, 2063–8 (2006).

[21]J. D. Breeze, J. M. Perkins, D. W. McComb, and N. M. Alford, "Do Grain Boundaries Affect Microwave Dielectric Loss in Oxides?" *J. Am. Ceram. Soc.*, **92**, 671–4 (2009). □